Chapter 10

White Matter Tracts Visualized by Parvalbumin in Nonhuman Primates

Kathleen Rockland

Additional information is available at the end of the chapter

http://dx.doi.org/10.5772/intechopen.70510

Abstract

A well-developed white matter (WM) is one of the characteristics of the primate brain. WM compartments ("tracts" or "bundles") are easily discernible by myelin or neurofilament stains, anterograde tracer injections in nonhuman primates (NHP), and, more recently, diffusion MRI. Relatively overlooked is the fact that several corticofugal and thalamocortical compartments and tracts can be visualized by immunohistochemistry (IHC) for calcium-binding proteins. Since this technique can be easily carried out on postmortem tissues, IHC for calcium-binding proteins is potentially an important bridge for comparisons between NHP and human tissues. This chapter attempts a brief overview of three WM tracts visualized by the calcium-binding protein parvalbumin (PV), as well as a description of the probable origin of the two corticofugal tracts; namely, from PV+ pyramidal cells. Furthermore, the complex, intertwining trajectory of callosal axons is illustrated by single axon reconstruction of five small groups of parietal cortical axons, anterogradely labeled by biotinylated dextran amine.

Keywords: axon trajectory, biotinylated dextran amine, calcium-binding proteins, calbindin-positive pyramidal neurons, corpus callosum, corticopontine tract, geniculocortical tract, parvalbumin-positive pyramidal neurons, single axon reconstruction

1. Introduction

The primate brain exhibits abundant species-specific specializations. Among others, it is gyrencephalic and has an appreciable amount of white matter. These features occur in other large brain species (for example, elephants, cetaceans, and large carnivores; cf.: http://brainmaps.org/) and are not in themselves defining features for primate brains. Nevertheless,

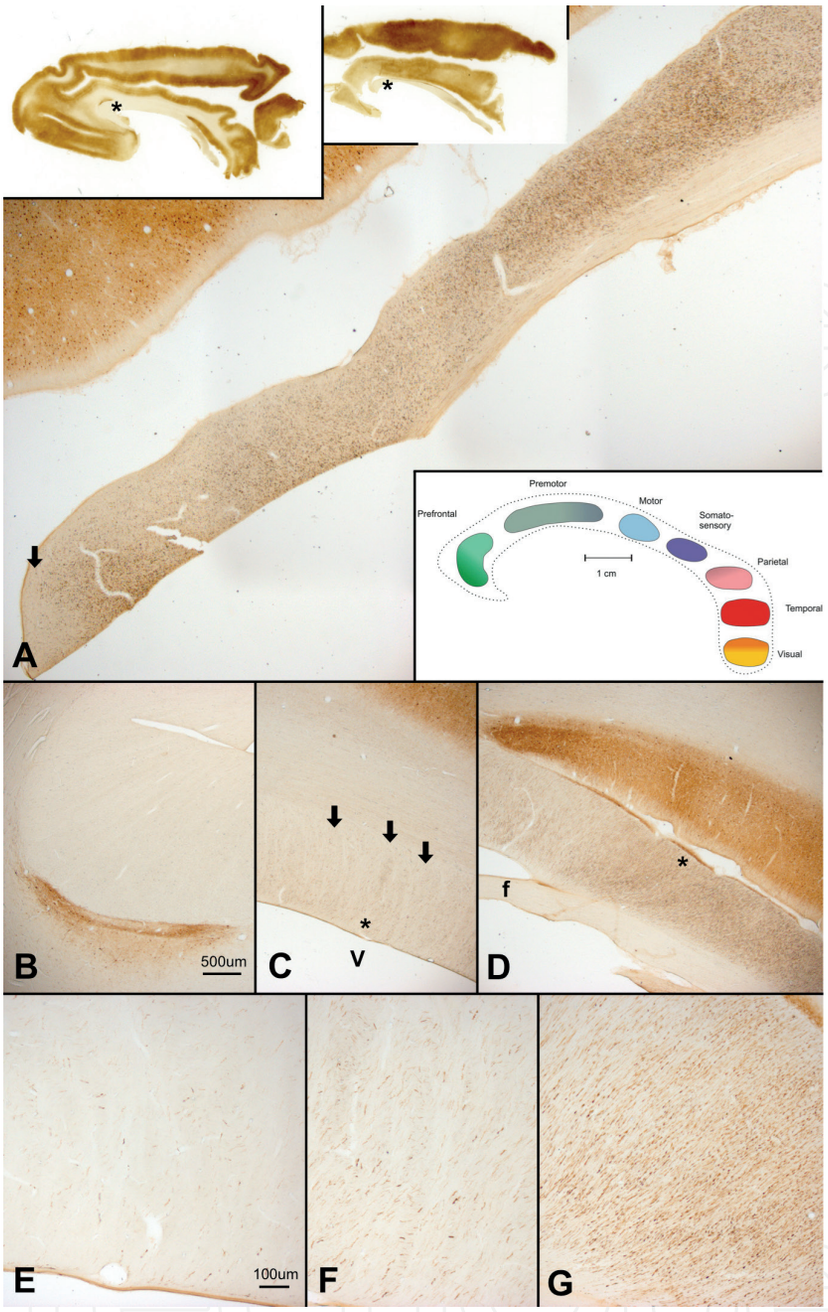

Figure 1. Sagittal sections of the corpus callosum in macaque monkey to illustrate PV+ fibers crossing in the corpus callosum. Anterior is to the left. (**A**) Low magnification overview near the mid-sagittal plane. Part of the anteroventral callosum was trimmed for a separate study, and the section is tilted from the horizontal plane for the sake of formatting. The density of PV+ fibers increases progressively from anterior to posterior. The zone of peak density corresponds to the territory of crossing premotor and motor axons (see schematic at lower right). The short arrow marks a distinct fall-off in density of PV+ fibers, anteriorly, in the vicinity of the rostrum (cut from the section). The histological sections at the upper left show the mediolateral planes of the fields illustrated in **A** (from the section at right), and **B–D** (from the section at left, which is 3.0 mm lateral to the midline). Asterisks = anterior corpus callosum. (**B–D**) Three photomicrographs sampling the anterior (**B**), middle (**C**), and posterior (**D**) regions of the corpus callosum (from the left histological section in **A**. Note increasing density of PV+ fibers with posterior progression. v = ventricle and f = fornix (devoid of PV+ fibers). The arrows in **C** point to three of the organized fascicles of PV+ fibers evident within the larger bundle. Asterisks in **C** and **D** indicate fields at a higher magnification in **F** and **G**. (**E–G**) Higher magnification from anterior (**E**), middle (**F**), and posterior (**G**) regions of the corpus callosum, showing increasing density of PV+ fibers. Scale bar in **B** applies to **A, C,** and **D**. Scale bar in **E** applies to **F, G**. Schematic inset in **A** is reproduced from [12]; Figure 1.

http://dx.doi.org/10.5772/intechopen.70510

they do usefully set apart primate brains from the lissencephalic and white matter-poor brains of rats and mice. Accordingly, this chapter focuses on several aspects of white matter (WM) organization in macaque monkeys.

The WM in primates has long been known to have suborganization and compartments ("tracts") (as reviewed in [1]). These have traditionally been identified on the basis of origin and target (for example, "corticospinal tract"). WM organization is most frequently investigated from classical myelin stains [2], diffusion MR imaging, and tractography (as reviewed in [3]), or, for nonhuman primates (NHP), labeled profiles after injection of anterograde tracers (as reviewed in [1]). Antibodies against neurofilaments (e.g., SMI32 or SMI312) can also be used [4]. Often overlooked is the fact that some WM tracts can effectively be visualized by immunohistochemistry (IHC) for calcium-binding proteins (calbindin, calretinin, or parvalbumin). These tracts include some callosally projecting axons and some corticofugal projections, originating from parvalbumin-positive (PV+) pyramidal neurons in motor and other cortical areas, as well as thalamocortical projections from PV+ thalamic projection neurons.

Importantly, visualization of neural structures by IHC for PV and the other calcium-binding proteins is a widely applicable technique and, in particular, can be used on immersion-fixed postmortem tissues. This is a definite advantage for morphofunctional investigations of human brains and allows (1) for easier extrapolation between human brains and those of the experimentally more accessible NHPs, (2) for assessment of neural changes between normal and abnormal conditions, and (3) for at least partial validation of tractography imaging data by the histological "gold standard."

This chapter focuses on three PV+ WM compartments (callosal, corticofugal, and thalamocortical) and the distribution of their likely cells of origin (see schematic in **Figure 1**). In addition, data from tracer injections relevant to the trajectory of callosal axons are included.

2. Methods

The data presented here are derived from four macaque brains histologically sectioned and reacted for PV, and two additional macaque brains with injections of the anterograde tracer biotinylated dextran amine (BDA) in inferior parietal cortex [5, 6]. Experimental protocols were all approved by the IACUC at the University of Iowa or the Animal Care Committee at RIKEN Institute (Wako-shi, Japan) and carried out in strict conformance with the NIH Guide for the care and use of laboratory animals (NIH Publication No. 80–23; revised 1996). Every effort was made to minimize the number of animals used and any pain or discomfort experienced by them. As a terminal step, animals were deeply anesthetized with ketamine (11 mg/kg, i.m.) and Nembutal (overdose, 75 mg/kg, i.p.) and were perfused transcardially, in sequence, with 0.9% saline containing 0.5% sodium nitrite, 4% paraformaldehyde in 0.1 M phosphate buffer (PB, 4 L over 30 minutes, pH 7.3), and chilled aliquots of 0.1 M PB with 10, 20, and 30% sucrose.

Brains were removed and, after equilibrating in 30% sucrose buffer, sectioned at 50 μm on a freezing microtome. For PV IHC [7], sections were incubated for 1 h in 0.1 M PB saline (PBS; pH 7.3) containing 0.5% Triton X-100 and 5% normal goat serum (PBS-TG) at room temperature and then for 40–48 h at 4°C with PBS-TG containing mouse monoclonal anti-PV antibody (Swant, Bellinzona, Switzerland; 1:50,000). After rinses, the sections were placed in PBS-TG containing biotinylated goat antimouse IgG (Vector Labs, 1:200) for 1.5 h at room temperature. Immunoreactivity was visualized by ABC incubation (one drop of reagent per 7 ml in 0.1 M PB; ABC Elite kits; Vector Labs) followed by diaminobenzidine (DAB) histochemistry with 0.03% nickel ammonium sulfate.

For the two monkeys with injections of the anterograde tracer BDA, surgery was carried out under sterile conditions after the animals were deeply anesthetized with barbiturate anesthesia (25 mg/kg Nembutal, i.v., following a tranquilizing dose of 11 mg/kg ketamine, i.m.). Parietal cortical areas of interest were localized by direct visualization, subsequent to craniotomy and durotomy, in relation to sulcal landmarks (i.e., the intraparietal and superior temporal sulci). Injections were made by pressure through a Hamilton syringe (10% BDA in 0.0125 M (PBS, 0.5–2.0 μl per injection); Molecular Probes, Eugene, Oregon).

Animals were allowed to recover and survived 18–29 days after injections. They were then reanesthetized, given an overdose of Nembutal (75 mg/kg), and perfused as described above. Brains were cut serially in the coronal plane by frozen microtomy (at 50 μm thickness) and processed histologically for BDA, as described in [5, 6]. Tissue was reacted for 20–24 h in avidin-biotin complex (ABC Elite kits; Vector Laboratories, Burlingame, California) at room temperature (one drop of reagent per 7 ml of 0.1 M PBS). In the final step, BDA was demonstrated by DAB histochemistry with the addition of 0.5% nickel-ammonium sulfate.

Regions of interest (ROIs) were digitized on a Zeiss Axiophot microscope using a 2.5×, 5×, or higher power objective. These high resolution images were then, if needed, stitched using the pairwise stitch function in Image J. Low magnification images of tissue sections were obtained by a high resolution flatbed scanner (Epson Perfection V700 Photo). Figures were assembled in GIMP or powerpoint and saved as JPEG (300 dpi). Axon reconstruction was carried out by camera lucida at low (5× objective) and higher magnifications (20× and 40× objectives).

3. Results

3.1. PV+ callosal axons

A subset of callosal axons in NHP is PV+, and this appears not to be the case for rat or mouse brains (**Figures 1–3**). The PV+ axons are evident through a large anterior-posterior (AP) extent of the callosum, but they are absent or sparse in the most anterior and most posterior portions (**Figure 1**). This corresponds to axons crossing between parts of prefrontal cortex (anteriorly) or early visual cortices (posteriorly), which are evidently PV−.

PV+ callosal fibers were consistently seen in all four brains, although staining in one brain was both fainter and more restricted in the AP extent, possibly suggesting intersubject variability in amount of PV expression. Inspection of online material (brainmaps.org for macaque and see [8] for human brain) confirms the occurrence of PV+ fibers in the WM and specifically in the callosum, although these seemed somewhat less abundant than in our material.

In the coronal plane of section, most fibers are cut in segments of short to intermediate lengths, as would be expected from coronal sectioning of fibers having an overall medial-lateral orientation and trajectory (**Figure 2**). At the light microscopic level, diameters vary from <1.0 to 2.0–4.0 μm. A previous analysis of BDA-labeled callosal fibers reported a range of 0.6–1.2 μm [9]. This study further found that the thickest axons originated from primary motor, somatosensory, and visual areas and the thinnest from prefrontal and temporal areas. Consistent with these findings, another investigation reports the majority of callosal axons as having a diameter of less than 1.0 μm [10], and an electron microscopic study of human and macaque brain also found average values below 1.0 μm [11].

Several papers have investigated fiber diameter, length, and trajectory, in part to evaluate impulse speed and conduction delay of callosal axons, in macaques and humans [10–12]. An early influential paper [13] used electron microscopy and IHC for glia to investigate and compare features of four cerebral commissures in macaque monkey. The increasing use of diffusion MR tractography, alone or in combination with stereology [14], offers an important new tool for WM analysis. The availability of a robust IHC marker, as described here for PV+ fibers, would facilitate comparisons across different age points, different conditions, and different species. Three-dimensional analysis, via serial sections or "clarified" tissue slabs, could easily reveal whether and how often branching occurs in the callosum and support quantification of axon diameters or clustering.

3.2. PV+ corticopontine tract

Other fiber tracts originating from PV+ corticofugal neurons (i.e., corticostriatal, corticorubral, or corticobulbar) are also identifiable by IHC. **Figure 4** documents PV+ corticostriatal and corticopontine fibers, and any number of images on the web (for human, see [8] and for macaque: http://brainmaps.org/index.php?action=viewslides&datid=22, see [4]) will show comparable PV+ tracts. Fibers in the corona radiata, immediately subjacent to motor cortex, contain a particularly dense PV+ population. Many of these are thick (6.0 μm in diameter) and exhibit a distinctive contorted geometry (**Figure 4**). Several surveys of fiber diameters have been published for corticofugal tracts [15–17].

An interesting question is whether the PV+ callosal connections are collateral branches of any of these corticofugal projections. In mice and rats, at least some corticostriatal neurons send collaterals to contralateral cortex [18], and contralateral corticostriatal projections have been described in [19]. Collateral branches from layer 5 neurons to thalamus and brainstem have been discussed in the context of links between perception and action ("efference copy") and may be another instance of primate specializations [20].

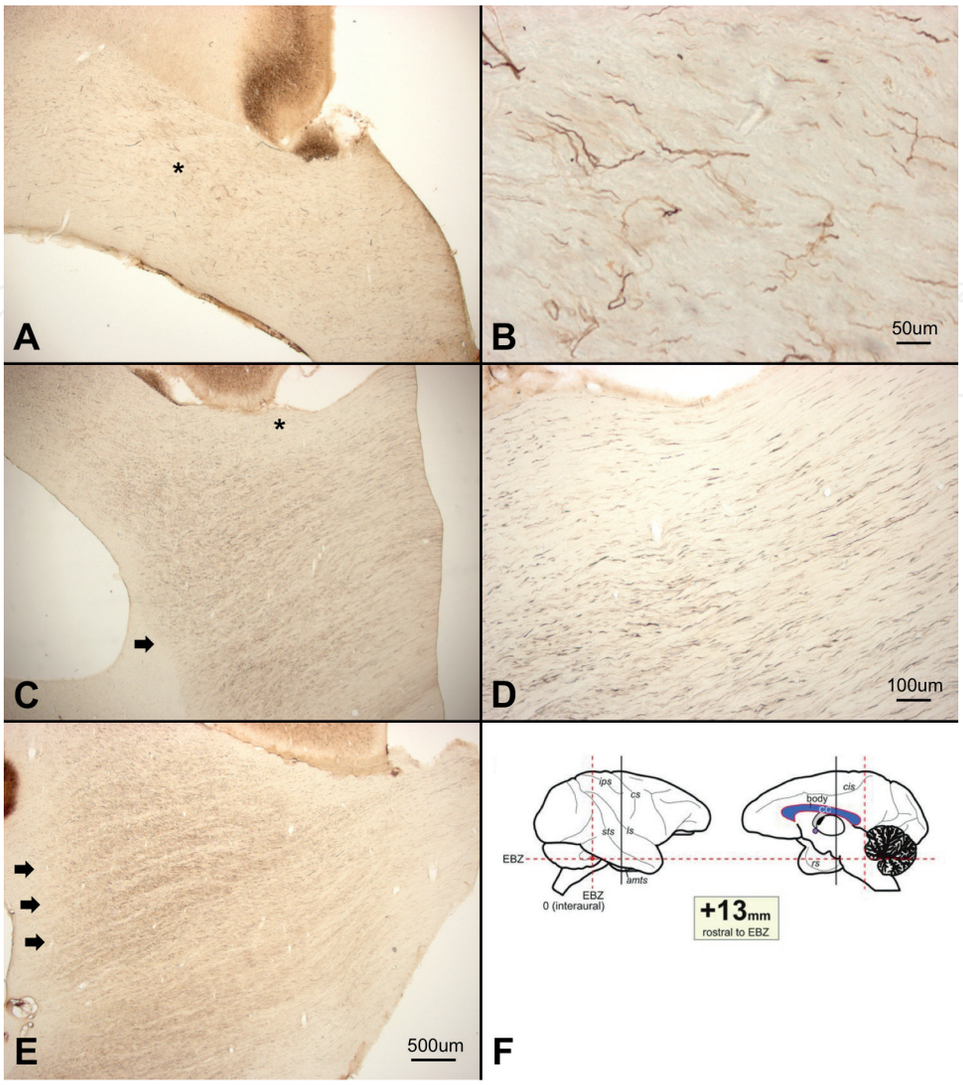

Figure 2. Coronal sections in macaque monkey to illustrate PV+ fibers crossing in the corpus callosum. Midline is to the right. (**A, C, E**) Anterior one-third, middle, and posterior AP levels, where **C** corresponds to the level of the solid vertical line in the right schematic hemisphere in **F**. Arrow in **C** calls attention to the sharp ventrolateral border of PV+ callosal fibers. Arrows in **E** highlight three of the fasciculations within the PV+ tract (see also **Figure 1C**). (**B** and **D**) Higher magnification from the regions of the asterisks in **A** and **C**. Note the scattered large fibers in **B** (and compare with the larger and more numerous large fibers in **Figure 4**). (**F**) Schematic of a right hemisphere, lateral, and medial surfaces (at the left and right of the schematic, respectively). The vertical lines indicate the coronal plane of section, with the more anterior, solid line corresponding to the level in **C**. The more posterior dashed line corresponds to the fields in **Figure 6** (and also the coronal histology section in **Figure 8C**). Reproduced from [4]; **Figure 6**. Scale bar in **E** applies to **A** and **C**.

3.3. PV+ cells of origin

PV is generally associated with subtypes of GABAergic, inhibitory interneurons, mainly basket and chandelier cells. While some GABAergic neurons have been reported to send axons through the corpus callosum [21], the numbers are small, much fewer than the number of PV+ callosal axons illustrated here.

A probable origin of the PV+ callosal fibers is the population of glutamatergic excitatory pyramidal neurons that co-label with PV (**Figures 5** and **6**). These include large Betz cells in layer

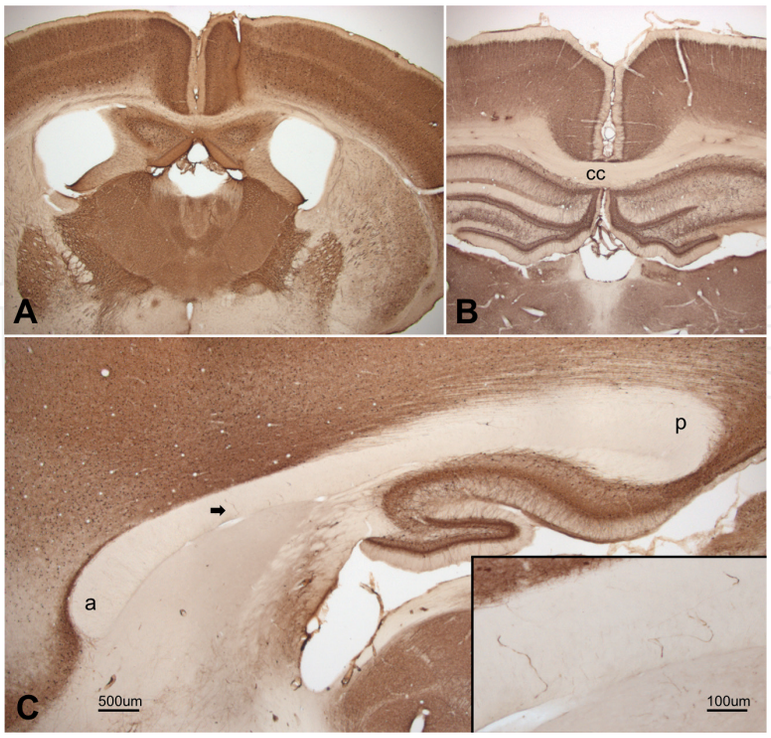

Figure 3. Photomicrographs of (**A**) a coronal section of mouse brain and (**B**) a coronal section of rat brain, both reacted for PV. Note the lack of PV+ fibers at the midline of the corpus callosum ("cc" in **B**). (**C**) Sagittal section through the corpus callosum in rat, slightly lateral to the midline. A few, scattered PV+ fibers are apparent (arrow, and at higher magnification: Inset). a = anterior and p = posterior. Scale bar in **C** applies to **A** and **B**.

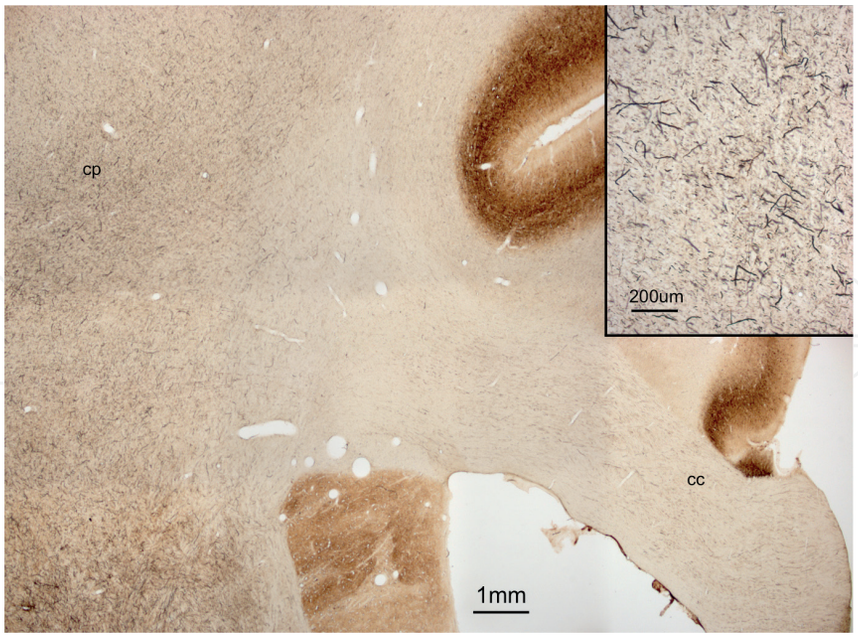

Figure 4. Dorsomedial segment of a coronal section (see solid vertical line in **Figure 2F**) to compare PV+ fibers in the corpus callosum (cc: at right) and those in the lateral white matter (coronal radiata and dorsal part of the internal capsule). The latter are subjacent to overlying motor cortex and partly correspond to corticopontine fibers (CP). CP fibers are thicker and often contorted (see higher magnification inset: upper right).

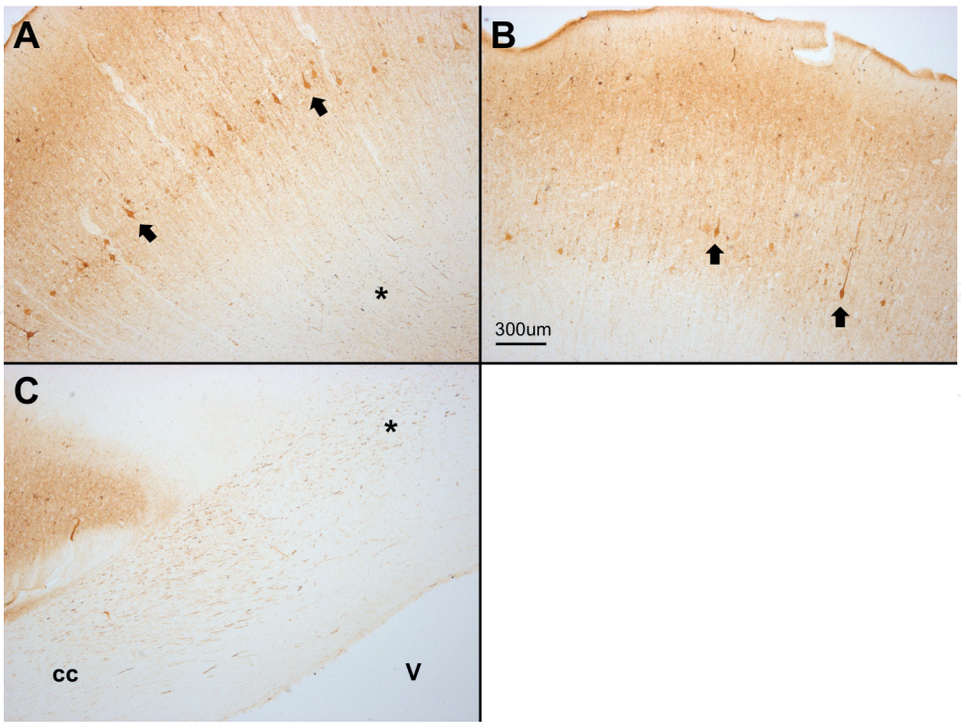

Figure 5. (**A** and **B**) PV+ Betz cells in motor cortex of macaque (coronal sections). Arrows point to two of the PV+ cells in each frame. PV+ interneurons and terminations are also evident. Asterisk in **A** highlights PV+ axons in the underlying white matter. AP level is slightly anterior to the solid vertical line in **Figure 2F**. (**C**) Another example, from the same brain, of PV+ fibers, putatively originating from the PV+ Betz cells in layer 5 and crossing in the corpus callosum (cc). Asterisk marks the callosal tract in a dorsolateral position, as it approaches the midline (at left in **C**). v = ventricle. Scale bar in **B** applies to **A–C**.

5 of motor cortex, large Meynert cells at the border of layers 5 and 6 of primary visual cortex, and large layer 5 pyramidal neurons in several other cortical areas [7, 22]. In histological sections of motor cortex, the PV+ pyramidal neurons typically measure 20 × 50, 30 × 40, or 20 × 30 μm. In the other areas, they can be as large as in motor cortex (i.e., 20 × 50 μm in the posterior cingulate) or toward the smaller range (20 × 30 μm), as in the parietal area 5 (**Figures 5** and **6**). These unusually PV+ pyramidal cells often have a more diffuse DAB filling (i.e., lighter brown) than adjacent PV+ interneurons, perhaps indicative of lower levels of PV (**Figure 6E**). The distribution of these neurons closely parallels that of corticospinal or corticopontine projecting neurons in frontal, premotor, and parietal areas, among others ([23, 24] and **Figure 7**). Thus, the question arises, as noted above, of whether at least some of the callosal connections could be collaterals of corticosubcortical projections originating from PV+ pyramidal cells.

For Betz and Meynert cells, these PV+ neurons also express the Kv3.1b potassium channel, which is usually associated with the fast-firing properties of PV+ interneurons [7, 25]. Physiological studies report that the PV+ pyramidal neurons in NHP exhibit short duration "thin spikes," in contrast to long-duration action potentials, characteristic of neurons in rat motor cortex [26]. The functional significance of this result has been discussed as relating to the fast-conducting property of macaque corticospinal neurons, with the conjecture that fast-conducting corticospinal

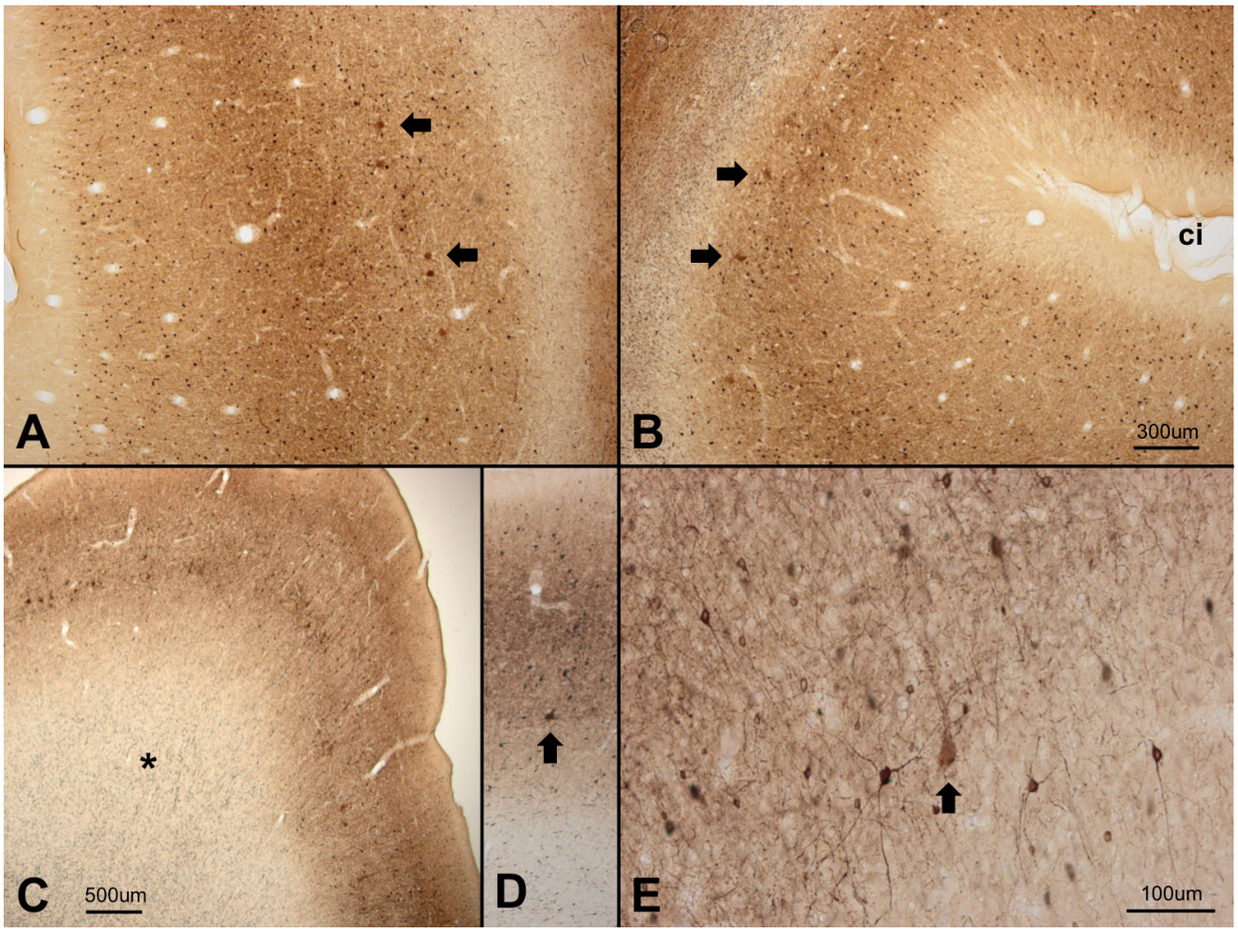

Figure 6. PV+ pyramidal neurons. These are the likely origins of PV+ callosal and/or corticosubcortical fibers. (**A**) A cluster of PV+ pyramidal neurons in layer 5, in the upper bank of the intraparietal sulcus. Arrows point to two of these. Medial is to the right (for **A–C**). (**B**) Arrows point to two of several PV+ pyramidal neurons in layer 5 at the depth of the cingulate sulcus (ci). (**C**) For comparison, a low magnification view from the same brain of PV+ Betz cells in motor cortex (approximately at the vertical dark line in **Figure 2F**). Asterisk marks PV+ fibers in the immediately subjacent white matter, probably corresponding to a mix of outgoing callosal and corticosubcortical fibers. (**D**) PV+ pyramidal neuron (arrow) in parietal area 5. **A, B**, and **D** are at approximately the same AP level as the dashed red line in **Figure 2F** (and see also coronal section in **Figure 8C**). (**E**) Higher magnification image of a PV+ pyramidal neuron (arrow) in a field of PV+ interneurons within the gray matter of the superior parietal lobule. Note lighter intensity of the PV stain for the pyramidal neuron. Scale bar in **B** applies to **A** and **D**.

neurons in macaque may make monosynaptic connections with the motoneurons innervating the most distal muscles controlling the fingers and toes (as discussed in [26]), and thus might be unique to dexterous primate species. This interpretation, however, does not readily apply to PV+ pyramidal neurons in areas outside motor cortex proper.

PV+ excitatory pyramidal neurons have been consistently reported in NHP [27] and, recently, in mice [28]. In PV-Cre transgenic mice, GFP-positive pyramidal neurons were found in layer 5 in a broad swath of cortical areas. In this preparation, the greatest number was in somatosensory cortex, but there were also PV+ pyramidal neurons in motor and visual areas. PV+ corticostriatal pyramidal neurons have been reported by co-labeling with retrograde tracers in mice. These were mainly in layer 5 of retrosplenial and somatosensory areas [29].

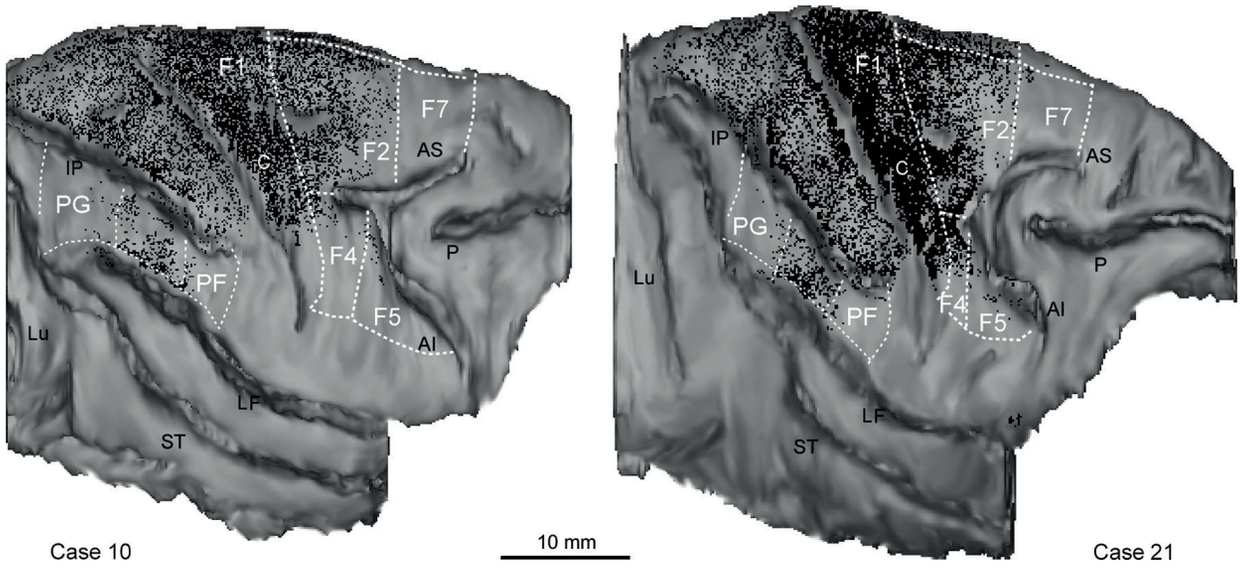

Figure 7. Distribution of retrogradely labeled neurons following retrograde tracer injections in the spinal cord at upper cervical levels (one dot = one neuron). Dorsolateral views of the cerebral hemispheres are shown for two brains (cases 10 and 21) contralateral to the injections. Reproduced from [24]; **Figure 15**.

3.4. Pyramidal cells positive for calbindin or calretinin

As a side observation, we should note that other CBPs are also expressed in subpopulations of glutamatergic cortical neurons, although with pronounced area and species differences [27, 30]. In rodents, there are numerous calbindin + (CB+) pyramidal neurons. CB+ pyramidal neurons are reported in NHP, mainly in the supragranular layers. In NHP, the density of CB+ pyramidal neurons has been described as an increasing gradient from primary visual cortex to temporal association areas [31], but, since a subpopulation of hippocampal CA1 pyramidal neurons is CB+ [32], in both rodents and NHPs, it could also be considered a *decreasing* density from CA1, through temporal association areas, to early and primary visual areas. Calretinin + pyramidal cells are reported in layer 5 of anterior cingulate cortex [27] and in deeper layers of entorhinal cortex in humans [33]. Fine analysis of CB+ or CR+ fiber tracts in NHP is lacking.

3.5. PV+ thalamocortical tract

The thalamocortical tract, including optic radiations (from the lateral geniculate nucleus to primary visual cortex), is a compact, well-delineated bundle in primates and can be readily identified even in classical myelin preparations (e.g., Figure 18-1 in [1]).

In primates, many thalamocortical projections are PV+. An influential distinction has been drawn between thalamocortical terminations that are PV+ and topographically organized vs. those that are CB+ and more diffuse ("core" and "matrix," respectively [34]), although this may hold for only a subdivision of thalamic nuclei. An extensive literature has confirmed that glutamatergic thalamic projection neurons co-localize with either PV or CB, and that their

cortical terminations can also be visualized by PV or CB [35, 36]. Relatively under-reported is the fact that the bundles of thalamocortical axons in their WM transit can also be visualized by CBP. This is immediately apparent in whole section atlases or histological images ("sste," external sagittal stratum or optic radiations) in Figures 7 and 17, and level 72b, 77b as in [8] and from Figures 16–23 in the horizontal plane as in [4]. **Figure 8** illustrates PV+ fibers in the thalamocortical tract in macaque (including the optic radiations). An obvious extension of this observation would be double IHC for CB and PV in the same histological preparation.

3.6. Intertwining callosal axons from parietal cortex

Interests in the corpus callosum has burgeoned in this epoch of MRI, and many studies have investigated the topographic organization and axon diameter distribution within the

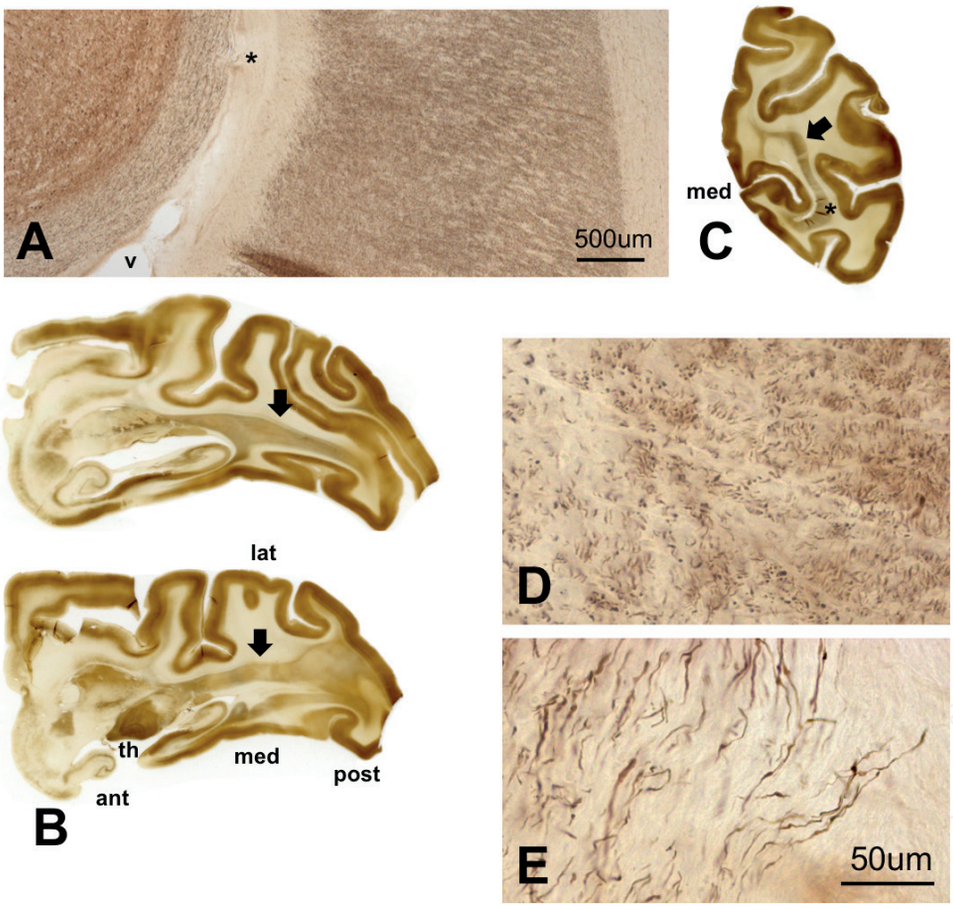

Figure 8. PV+ fibers in the thalamocortical tract. (**A**) Low magnification of the asterisk in **C**, which shows a coronally sectioned histological section. Medial (med) is to the left. Obliquely sectioned geniculocortical axon segments in **A** are subjacent to primary visual cortex. These have exited from the larger, more lateral thalamocortical tract. (**B**) PV+ thalamocortical tract is clearly evident in two horizontally sectioned tissue sections (The upper section is more ventral, and both are below the corpus callosum.) Arrows in **B** and **D** identify the PV+ thalamocortical tract. (**D** and **E**) Higher magnification of the asterisk in **A**, showing detail and different orientation of PV+ fibers. The thalamocortical tract takes a predominantly AP trajectory, so that the coronal plane of section results in fibers cut almost in cross-section. v = ventricle, ant = anterior, lat = lateral, post = posterior, and th = thalamus. Scale bar in **D** applies to **E**.

corpus callosum, both by histological [9–11] and imaging [11, 12] approaches. The trajectory of individual axons, as visualized at high resolution, has been relatively unaddressed. However, serial section analysis (about technique, see [37]) through small segments of the callosum (1.0–2.0 mm AP) reveals that fibers take a complicated, shifting trajectory. **Figure 9** shows five groups of callosal axons (n = 3–5) anterogradely labeled by an injection of BDA in parietal areas (areas 5 or 7) in NHP (see coronal sections at right for orientation). When followed through a reconstructed 3D space (5.4–6.4 mm ML and 2.2–2.8 mm AP), these can be seen to intertwine and exchange dorsoventral position. The "intertwining" (hollow arrows) is within a histological section of 50 μm thickness. At some points (solid arrows), the intertwining is within the same focal plane, compatible with the possibility of physical axon-axon contact.

The principle conclusion from this result is that individual axons do not maintain a stereotyped position but rather shift position within 3D space. An additional conclusion is that closely adjacent axons do not necessarily travel in a parallel trajectory but can intertwine. Similar reconstructions are not available for rodent.

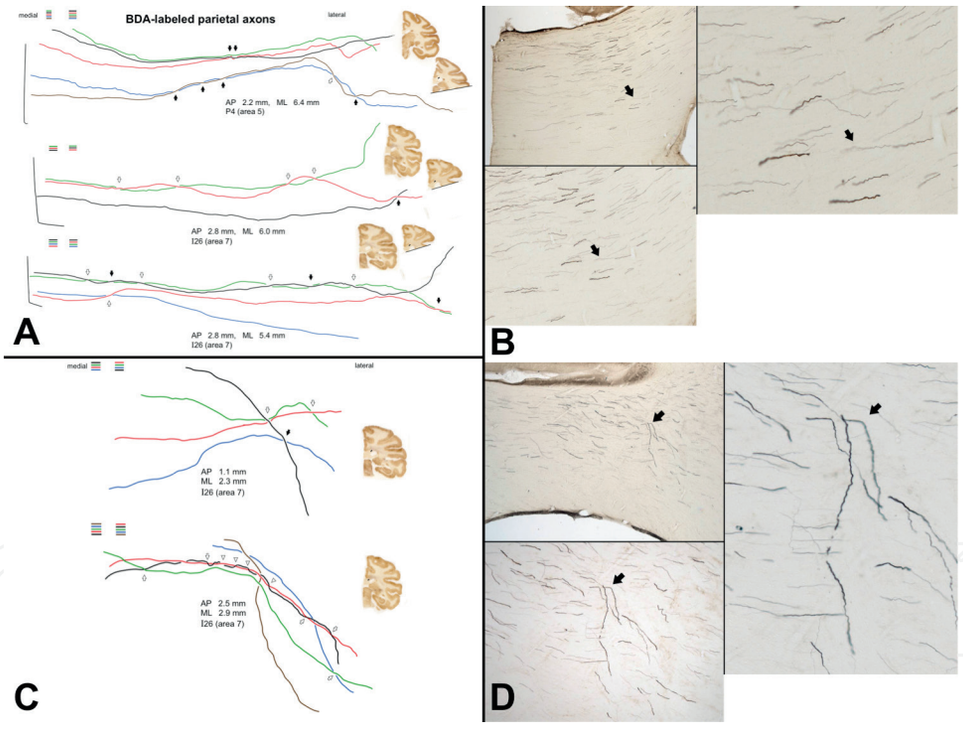

Figure 9. (**A** and **C**) Serial section reconstruction of five groups of parietal callosal axons (consisting of 5, 3, and 4 axons in **A** and 4 and 5 axons in **B**, anterogradely labeled by BDA). As shown for each of the five groups, axons were followed for 1.1–2.8 mm AP and 2.3–6.6 mm ML (mediolateral). Case P4 had a tracer injection in area 5, and case I26 had a large tracer injection in the inferior parietal lobule (area 7). Medial and the cut edge of the corpus callosum are at the left. By color coding the individual axons, it becomes apparent that the order is shuffled, even over these relatively short distances. The medialmost and lateralmost positions of the individual axons are summarized in the color boxes, at upper left for the five axon groups. Small histology sections at the right indicate the AP level of the reconstructions. Intertwinings of individual axons are indicated by solid arrows or, if the crossings occur in the same focal plane, hollow arrows. (**B** and **D**) Histological images corresponding to one coronal histology section (i.e., one AP level) of the axon reconstructions. Arrows point to regions depicted at progressively higher magnification in the three photomicrographs in **B** and **D**.

4. Conclusions

The large, gyrencephalic brains of primates are associated with a well-developed white matter. This has its own organization, in part based on identifiable bundles of axons connecting specific source and target areas. This is increasingly investigated by diffusion MR, although the accuracy of relationships between anatomical substrates and imaging data is still being determined [3, 12, 14]. The white matter also has neurochemically distinct elements. Some of these—the great transmitter-defined glutamatergic, GABAergic, or neuromodulatory fiber tracts—persist across species, although probably with quantifiable species-specific specializations. In primates, as discussed in this chapter, subsystems are characterized by co-localization with PV and other calcium-binding proteins. Callosal and corticofugal PV+ fibers originate from PV+ cell bodies in motor and other cortical areas. PV+ thalamocortical fibers originate from PV+ subpopulations of thalamic neurons. The current interpretation, supported by evidence from the corticospinal tract, is that PV+ excitatory cortical neurons (which are often coincident with neurons positive for the KV3.1b potassium channel) have fast firing properties such as might be needed for fine motor dexterity. Since IHC for PV can be easily carried out in postmortem tissues, this provides a useful morphological label across primate species.

Acknowledgements

I thank Andrew Chang for assistance with figures and manuscript preparation and Dr. Haiyan Gong for the use of her flatbed scanner. Dr. Marie Wintzer (RIKEN Brain Research Institute) contributed substantially to the axon reconstructions in **Figure 9** (Section 3.6).

Author details

Kathleen Rockland

Address all correspondence to: krock@bu.edu

Department of Anatomy and Neurobiology, Boston University School of Medicine, Boston, Massachusetts, United States

References

[1] Schmahmann JD, Pandya DN. Fiber Pathways of the Brain. New York: Oxford University Press; 2006

[2] Dejerine JJ. Anatomie des Centres Nerveux. Paris: Rueff et Cie; 1895

[3] Wandell BA. Clarifying human white matter. Annual Review of Neuroscience. Jul 8, 2016;**39**:103-128

[4] Saleem KS, Logothetis NK. A Combined MRI and Histology Atlas of the Rhesus Monkey Brain in Sterotaxic Coordinates. 2nd ed. San Diego: Elsevier/Academic Press; 2012

[5] Ding S-L, Van Hoesen G, Rockland KS. Inferior parietal lobule projections to the presubiculum and neighboring ventromedial temporal cortical areas. The Journal of Comparative Neurology. 2000 Oct 2;**425**(4):510-530

[6] Zhong Y-M, Rockland KS. Inferior parietal lobule projections to anterior inferotemporal cortex (area TE) in macaque monkey. Cerebral Cortex. 2003 May;**13**(5):527-540

[7] Ichinohe N, Watakabe A, Miyashita T, Yamamori T, Hashikawa T, Rockland KS. A voltage-gated potassium channel, Kv3.1b, is expressed by a subpopulation of large pyramidal neurons in layer 5 of the macaque monkey cortex. Neuroscience. 2004;**129**(1):179-185

[8] Ding S-L, Royall JJ, Sunkin SM, Ng L, Facer BAC, Lesnar P, et al. Comprehensive cellular-resolution atlas of the adult human brain. The Journal of Comparative Neurology. Nov 1, 2016;**524**(16):3127-3481

[9] Tomasi S, Caminiti R, Innocenti GM. Areal differences in diameter and length of corticofugal projections. Cerebral Cortex. 2012 Jun;**22**(6):1463-1472

[10] Phillips KA, Stimpson CD, Smaers JB, Raghanti MA, Jacobs B, Popratiloff A, et al. The corpus callosum in primates: Processing speed of axons and the evolution of hemispheric asymmetry. Proceedings of the Biological Sciences. Nov 7, 2015;**282**(1818):20151535

[11] Liewald D, Miller R, Logothetis N, Wagner H-J, Schüz A. Distribution of axon diameters in cortical white matter: An electron-microscopic study on three human brains and a macaque. Biological Cybernetics. Oct 2014;**108**(5):541-557

[12] Caminiti R, Carducci F, Piervincenzi C, Battaglia-Mayer A, Confalone G, Visco-Comandini F, et al. Diameter, length, speed, and conduction delay of callosal axons in macaque monkeys and humans: Comparing data from histology and magnetic resonance imaging diffusion tractography. The Journal of Neuroscience. Sep 4, 2013;**33**(36):14501-14511

[13] Lamantia AS, Rakic P. Cytological and quantitative characteristics of four cerebral commissures in the rhesus monkey. The Journal of Comparative Neurology. Jan 22, 1990;**291**(4): 520-537

[14] Charvet CJ, Hof PR, Raghanti MA, Van Der Kouwe AJ, Sherwood CC, Takahashi E. Combining diffusion magnetic resonance tractography with stereology highlights increased cross-cortical integration in primates. The Journal of Comparative Neurology. Apr 1, 2017;**525**(5):1075-1093

[15] Morecraft RJ, McNeal DW, Stilwell-Morecraft KS, Dvanajscak Z, Ge J, Schneider P. Localization of arm representation in the cerebral peduncle of the non-human primate. The Journal of Comparative Neurology. Sep 10, 2007;**504**(2):149-167

[16] Firmin L, Field P, Maier MA, Kraskov A, Kirkwood PA, Nakajima K, et al. Axon diameters and conduction velocities in the macaque pyramidal tract. Journal of Neurophysiology. Sep 15, 2014;**112**(6):1229-1240

[17] Innocenti GM, Vercelli A, Caminiti R. The diameter of cortical axons depends both on the area of origin and target. Cerebral Cortex. Aug 2014;**24**(8):2178-2188

[18] Shepherd GMG. Corticostriatal connectivity and its role in disease. Nature Reviews. Neuroscience. Apr 2013;**14**(4):278-291

[19] Innocenti GM, Dyrby TB, Andersen KW, Rouiller EM, Caminiti R. The crossed projection to the striatum in two species of monkey and in humans: Behavioral and evolutionary significance. Cerebral Cortex. Jun 9, 2016:3217-3230. DOI: 10.1093/cercor/bhw161

[20] Guillery RW. Anatomical pathways that link perception and action. Progress in Brain Research. 2005;**149**:235-256

[21] Peters A, Payne BR, Josephson K. Transcallosal non-pyramidal cell projections from visual cortex in the cat. The Journal of Comparative Neurology. Dec 1, 1990;**302**(1):124-142

[22] Preuss TM, Kaas JH. Parvalbumin-like immunoreactivity of layer V pyramidal cells in the motor and somatosensory cortex of adult primates. Brain Research. Mar 18, 1996; **712**(2):353-357

[23] Geyer S, Matelli M, Luppino G, Zilles K. Functional neuroanatomy of the primate isocortical motor system. Anatomy and Embryology. Dec 2000;**202**(6):443-474

[24] Rozzi S, Calzavara R, Belmalih A, Borra E, Gregoriou GG, Matelli M, et al. Cortical connections of the inferior parietal cortical convexity of the macaque monkey. Cerebral Cortex. Oct 2006;**16**(10):1389-1417

[25] Constantinople CM, Disney AA, Maffie J, Rudy B, Hawken MJ. Quantitative analysis of neurons with Kv3 potassium channel subunits, Kv3.1b and Kv3.2, in macaque primary visual cortex. The Journal of Comparative Neurology. Oct 1, 2009;**516**(4):291-311

[26] Soares D, Goldrick I, Lemon RN, Kraskov A, Greensmith L, Kalmar B. Expression of Kv3.1b potassium channel is widespread in macaque motor cortex pyramidal cells: A histological comparison between rat and macaque. The Journal of Comparative Neurology. Feb 18, 2017:2164-2176. DOI: 10.1002/cne.24192

[27] Hof PR, Glezer II, Condé F, Flagg RA, Rubin MB, Nimchinsky EA, et al. Cellular distribution of the calcium-binding proteins parvalbumin, calbindin, and calretinin in the neocortex of mammals: Phylogenetic and developmental patterns. Journal of Chemical Neuroanatomy. 1999 Feb;**16**(2):77-116

[28] Tanahira C, Higo S, Watanabe K, Tomioka R, Ebihara S, Kaneko T, et al. Parvalbumin neurons in the forebrain as revealed by parvalbumin-Cre transgenic mice. Neuroscience Research. Mar 2009;**63**(3):213-223

[29] Jinno S, Kosaka T. Parvalbumin is expressed in glutamatergic and GABAergic corticostriatal pathway in mice. The Journal of Comparative Neurology. Sep 13, 2004;**477**(2):188-201

[30] Suzuki WA, Porteros A. Distribution of calbindin D-28k in the entorhinal, perirhinal, and parahippocampal cortices of the macaque monkey. The Journal of Comparative Neurology. Sep 30, 2002;**451**(4):392-412

[31] Kondo H, Tanaka K, Hashikawa T, Jones EG. Neurochemical gradients along monkey sensory cortical pathways: Calbindin-immunoreactive pyramidal neurons in layers II and III. The European Journal of Neuroscience. Dec 1999;**11**(12):4197-4203

[32] Mizuseki K, Diba K, Pastalkova E, Buzsáki G. Hippocampal CA1 pyramidal cells form functionally distinct sublayers. Nature Neuroscience. Aug 7, 2011;**14**(9):1174-1181

[33] Mikkonen M, Soininen H, Pitkänen A. Distribution of parvalbumin-, calretinin-, and calbindin-D28k-immunoreactive neurons and fibers in the human entorhinal cortex. The Journal of Comparative Neurology. Nov 10, 1997;**388**(1):64-88

[34] Jones EG. Viewpoint: The core and matrix of thalamic organization. Neuroscience. Jul 1998;**85**(2):331-345

[35] DeFelipe J, Jones EG. Parvalbumin immunoreactivity reveals layer IV of monkey cerebral cortex as a mosaic of microzones of thalamic afferent terminations. Brain Research. Oct 18, 1991;**562**(1):39-47

[36] Melchitzky DS, Sesack SR, Lewis DA. Parvalbumin-immunoreactive axon terminals in macaque monkey and human prefrontal cortex: Laminar, regional, and target specificity of type I and type II synapses. The Journal of Comparative Neurology. May 24, 1999;**408**(1):11-22

[37] Rockland KS. Visual cortical organization at the single axon level: A beginning. Neuroscience Research. Mar 2002;**42**(3):155-166